INSTITUTE OF PHYSICS PUBLISHING JOURNAL OF PHYSICS D: APPLIED PHYSICS
J. Phys. D: Appl. Phys. **39** (2006) 1866–1871 doi:10.1088/0022-3727/39/9/022

Electron drift velocity in N_2O in strong electric fields determined from rf breakdown curves

V Lisovskiy[1,3], J-P Booth[1], K Landry[2], D Douai[2], V Cassagne[2] and V Yegorenkov[3]

[1] Laboratoire de Physique et Technologie des Plasmas, Ecole Polytechnique, Palaiseau 91128, France
[2] Displays Division, Unaxis France SA, 5 Rue Leon Blum, Palaiseau 91120, France
[3] Department of Physics and Technology, Kharkov National University, Kharkov 61077, Ukraine

E-mail: lisovskiy@yahoo.com

Received 11 January 2006, in final form 6 March 2006
Published 20 April 2006
Online at stacks.iop.org/JPhysD/39/1866

Abstract
We report measurements of the breakdown curves of an rf capacitive discharge in low pressure nitrous oxide. The electron drift velocity was determined from the locations of the turning point and of the minimum in the breakdown curves in the range $E/p = 87$–$840\ \mathrm{V\,cm^{-1}\,Torr^{-1}}$. We compare our results with values calculated from the published cross-sections in the range $E/p = 1$–$5000\ \mathrm{V\,cm^{-1}\,Torr^{-1}}$ and find good agreement.

1. Introduction

RF discharges in N_2O are used in many applications including removing hydrocarbon impurities from silicon wafers, oxidizing silicon surfaces [1] and creating silicon oxynitride films on silicon [2]. RF discharges in $N_2O + SiH_4$ mixtures are used for depositing amorphous oxynitrides films (a-SiN_xO_y and a-SiN_xO_y : H) [3–7]. In a number of cases rf discharges in $N_2O + SiH_4$ mixtures are used to deposit SiO_2 films [8–12]. Typically the N_2O concentration in the $N_2O + SiH_4$ mixture is 2–40 times higher than that of silane. Consequently it is of considerable interest to study the properties of rf capacitive discharges and electron transport parameters in pure N_2O.

In order to use fluid simulations it is necessary to know the electron transport parameters of the gas under study. Electron swarm motion through gases is described by the following parameters: the electron drift velocity, V_{dr}, the first Townsend coefficient, α, the rate of electron attachment to gas molecules, η, the average electron energy, $\langle\varepsilon_e\rangle$, and the ratio of radial electron diffusion coefficient to mobility, D_e/μ_e. To our knowledge, these transport parameters have only been measured in N_2O for small values of the reduced electric field ($E/p < 174\ \mathrm{V\,cm^{-1}\,Torr^{-1}}$ [13–20]). However the reduced field, E/p, may reach hundreds of $\mathrm{V\,cm^{-1}\,Torr^{-1}}$ in the near-electrode sheaths of rf discharges, in the cathode sheath of dc discharges, during a gas breakdown and in a number of other cases. Under these conditions the electrons can acquire considerable energy, and therefore it is necessary to know the electron transport parameters in these strong electric fields.

The electron drift velocity in an electric field, V_{dr}, characterizes the conductivity of a weakly ionized gas and is one of the most important electron transport parameters. There are a number of well-known techniques (the time-of-flight technique, observation of the optical radiation of a moving electron swarm, the shutter technique and so on) that have been used to measure the electron drift velocity. However, these only work for comparatively small reduced fields, E/p, because at higher values a self-sustaining discharge is ignited which impedes the measurement. Lisovskiy and co-workers [21–24] have used a novel method to determine the electron drift velocity from the location of the turning point in the breakdown curves of rf capacitive discharges. In addition Lisovskiy *et al* [25] proposed a new technique for determining V_{dr} from the location of the minimum in the rf breakdown curve and applied it to argon, ammonia, nitrogen, hydrogen and oxygen. Whereas conventional techniques become inapplicable after the ignition of the self-sustaining discharge, these two methods are actually based on discharge ignition, allowing measurements of V_{dr} in strong electric fields.

In this paper we have used these techniques to determine the electron drift velocity in N_2O. Measurements were made

in the range $E/p = 87$–$840\,\mathrm{V\,cm^{-1}\,Torr^{-1}}$. With the help of the 'Bolsig' numerical code and published cross-sections [26] we have calculated the electron transport parameters in N_2O in the range $E/p = 1$–$5000\,\mathrm{V\,cm^{-1}\,Torr^{-1}}$, and the drift velocity values obtained from our experiment agree well with the calculated values.

2. Experimental set-up

The rf discharge was ignited in N_2O over the pressure range $p \approx 0.05$–17 Torr with rf field frequencies $f = 2$ MHz, $f = 13.56$ MHz and $f = 27.12$ MHz. The distance between the flat circular aluminium electrodes (143 mm in diameter) was varied over the range $L = 2$–27 mm. RF voltage (amplitude $U_{\mathrm{rf}} < 1500$ V) was fed to one of the electrodes, while the other was grounded. The electrodes were located inside a fused silica tube with an inner diameter of 145 mm (see figure 1). The gas was supplied through small orifices in the powered electrode and then pumped out via the gap between the second electrode and the wall of the fused silica tube.

The gas pressure was monitored with 10 and 1000 Torr capacitive manometers (MKS Instruments). The gas flow was fixed with a mass flow controller to 5 sccm and the pressure regulated by throttling the outlet to the pump. The rf voltage was measured with an rf current–voltage probe (Advanced Energy Z'SCAN).

We used the technique proposed by Levitskii [27] to measure the rf breakdown curves. Near and to the high pressure side of the minimum in the breakdown curve, the N_2O pressure was fixed before slowly increasing the rf voltage until gas breakdown occurs. To the low pressure side of the minimum the curve may be multi-valued, i.e. the curve turns around and breakdown occurs at two different values of the rf voltage. Therefore in this range we first decreased the N_2O pressure, then fixed the rf voltage value and only then increased the N_2O pressure slowly until discharge ignition occurred. When discharge ignition occurs the rf voltage decreases sharply, and a glow appears between the electrodes indicating the onset of gas breakdown. The uncertainty in the measured breakdown voltages did not exceed 1–2 V over the whole U_{rf} range under study.

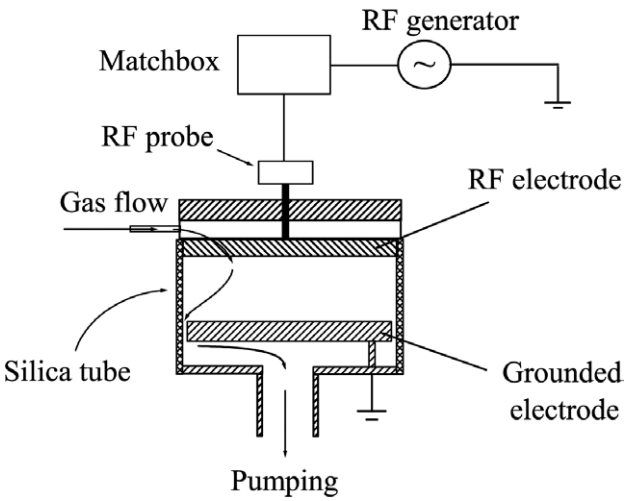

Figure 1. Schematic of the experimental setup.

3. Experimental results

3.1. Breakdown curves in N_2O

The breakdown curves of rf capacitive discharges can be divided into different branches according to the processes by which the charged particles are generated: emission-free, diffusion–drift, Paschen and multipactor branches, as described in detail elsewhere [22].

Figure 2(*a*) shows the rf breakdown curves determined with a frequency $f = 13.56$ MHz and a range of inter-electrode gap values, L. With $L = 25$ mm the breakdown curve possesses a diffusion-drift branch with a clearly-expressed region of multi-valued dependence of the rf breakdown voltage on gas pressure (at low gas pressure), as well as the emission-free branch (at high pressure, $p > 1$ Torr). The Paschen and multipactor branches were not observed with this large inter-electrode gap.

Decreasing the inter-electrode gap, L, shifts the diffusion-drift branch towards higher rf voltages and gas pressures. At the same time a section of the Paschen branch appears in the low pressure region (to the left of the breakdown curve minimum). For example, with $L = 13.5$ mm the Paschen branch appears in the low pressure region for voltages, $U_{\mathrm{rf}} > 350$ V: in this region the breakdown voltage increases as the pressure is decreased. Decreasing the gap, L, reduces the range of the multi-valued region, and it disappears when $L < 12$ mm. Further decrease in the inter-electrode gap leads to the disappearance of the diffusion-drift branch (in the breakdown curve for $L = 6$ mm the diffusion-drift branch appears only at gas pressures, $p > 7$ Torr), and at low

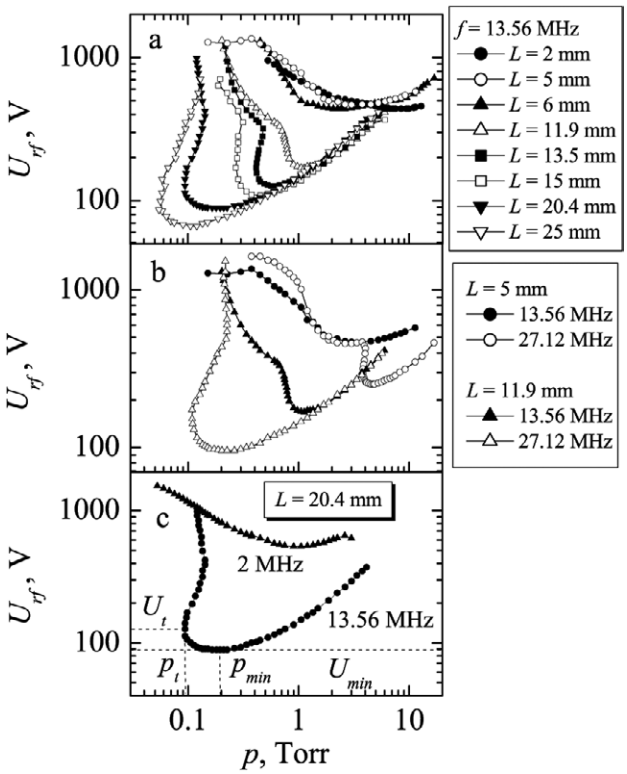

Figure 2. RF discharge breakdown curves in N_2O for different inter-electrode gap values and frequencies.

gas pressures and high rf voltages a multipactor branch is observed (a section with practically constant rf breakdown voltage, seen for example with $L = 5$ mm and gas pressures $p < 0.4$ Torr).

It should be remarked that these features (a multi-valued section, Paschen and multipactor branches at low gas pressure) are only observed in symmetric rf discharges [28], i.e. the planar electrodes must be situated inside a dielectric tube with an inner diameter close to the outer diameter of the electrodes. If the electrodes are located inside a grounded chamber of larger dimensions and their radial boundary is not limited with a dielectric tube then the rf breakdown curve will not possess these features [28, 29].

Let us now discuss how the rf field frequency affects the shape of breakdown curves. Figure 2(*b*) presents breakdown curves for inter-electrode gaps of $L = 5$ mm and $L = 11.9$ mm and frequencies $f = 13.56$ MHz and $f = 27.12$ MHz. The breakdown curves for $L = 11.9$ mm possesses no multi-valued region in the low pressure range for $f = 13.56$ MHz, whereas a wide multi-valued region is seen for $f = 27.12$ MHz. In the high pressure region the breakdown curves for both frequencies coincide, in agreement with previous studies [30, 31] which have shown that the rf breakdown voltage is independent of the frequency at high pressure. The breakdown curve for $L = 5$ mm and $f = 13.56$ MHz possesses no diffusion-drift branch, consisting of the Paschen branch with multipactor branch at low pressure. However, with $f = 27.12$ MHz (keeping $L = 5$ mm) we see a diffusion–drift branch with a small multi-valued region and in the low pressure region a Paschen branch and a multipactor branch. We could not record the curve over the entire multipactor region for $L = 5$ mm and $f = 27.12$ MHz due to a technical problem, but the behaviour of the curves for $L = 5$ mm and $f = 13.56$ MHz and $f = 27.12$ MHz shows that increasing the frequency of the rf electric field leads to an increase in the ignition voltage in the multipactor regime, in agreement with previous papers [32–35].

Figure 2(*c*) shows the effect of changing the frequency from $f = 13.56$ to 2 MHz with $L = 20.4$ mm. The curve for $f = 13.56$ MHz possesses a diffusion–drift branch with a multi-valued region as well as part of the Paschen branch. The curve for $f = 2$ MHz consists almost entirely of the Paschen branch. Only at low N_2O pressure is the beginning of the transition to the multipactor branch observed, and the last recorded point at high gas pressure may show the beginning of the transition to the diffusion–drift branch.

Up to now no similarity law has been proposed for rf breakdown curves, even for a single rf frequency. For dc discharges Paschen's law [36, 37] states that the breakdown voltage depends only on the value of the product pL. However, figure 3 shows that for rf breakdown, in the high pressure range (to the right of the breakdown curve minima), this does not hold, and the breakdown voltage is found to decrease approximately linearly as L is increased. Figure 4 shows breakdown curves for different gaps, L, plotted as a function of the product pL instead of simply pressure. However, this does not lead to convergence of the diffusion-drift branches recorded for different gap values, except for the sections of Paschen branches near and to the right of their minima for small gaps ($L \leqslant 6$ mm). However, in the low pressure range (to the

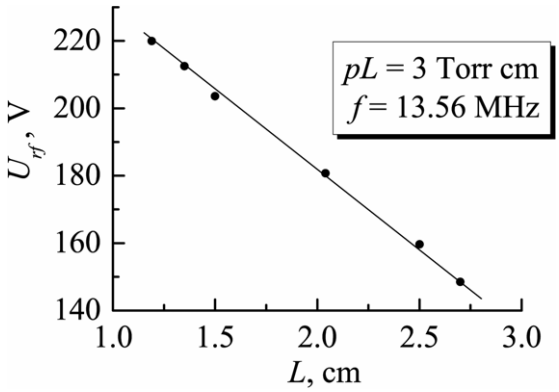

Figure 3. Breakdown rf voltage against inter-electrode gap value for $f = 13.56$ MHz $pL = 3$ Torr cm.

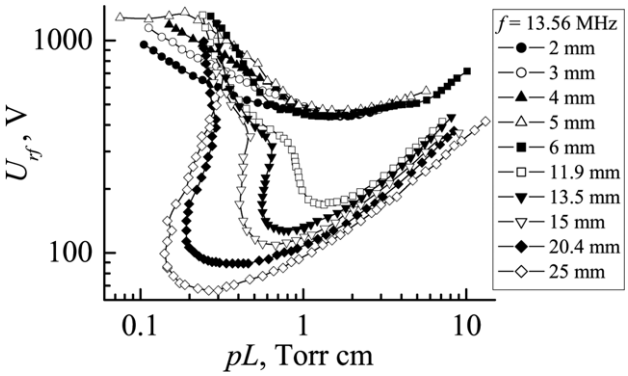

Figure 4. Breakdown curves for $f = 13.56$ MHz and different gap values, plotted as a function of the product pL.

left of minima) the Paschen branches for different gap values diverge. The breakdown curves for microwave discharges have been found to obey the similarity law $E\Lambda = \psi(p\Lambda)$ [38], where $E_{rf} = U_{rf}/L$ is the rf electric field strength and Λ is the diffusion length of the discharge chamber (of length L and radius R) given by the relation

$$\frac{1}{\Lambda^2} = \left(\frac{2.405}{R}\right)^2 + \left(\frac{\pi}{L}\right)^2. \qquad (1)$$

However, when our data is plotted in this way the curves do not superpose, and this law appears to be inapplicable for rf gas breakdown (at least for N_2O).

Thus, as is clear from figure 2(*c*), the breakdown curve for $L = 20.4$ mm (as well as some of the other breakdown curves presented in figure 2) possesses a region of multi-valued dependence of the rf breakdown voltage on gas pressure [21–25, 27, 28, 39], i.e. at certain given gas pressures the rf discharge can be ignited at two and even three different values of the rf voltage (e.g. in the N_2O pressure range $p \approx 0.12$–0.14 Torr in figure 2(*c*)). The diffusion-drift branch shows a well-expressed turning point with the coordinates $p = p_t$ and $U_{rf} = U_t$. For the conditions corresponding to the turning point the amplitude of the electron displacement in the rf field is equal to one-half of the inter-electrode gap value, as discussed below.

3.2. Electron drift velocity determination from rf breakdown curves in N_2O

Let us consider the equation of motion for the electron velocity, $\vec{V}$, in a uniform rf electric field:

$$m\frac{\mathrm{d}\vec{V}}{\mathrm{d}t} = -e\vec{E}_{\mathrm{rf}}\sin\omega t - m\vec{V}\nu_{\mathrm{en}}, \tag{2}$$

where e and m are the electron charge and mass, respectively, E_{rf} is the rf field amplitude, ν_{en} is the effective frequency of collisions between electrons and gas molecules and $\omega = 2\pi f$ is the angular frequency of the rf field. By integrating (2) and the equation for oscillatory motion, $\mathrm{d}\vec{r}/\mathrm{d}t = \vec{V}$, we find

$$\vec{V} = \frac{e\vec{E}_{\mathrm{rf}}}{m\sqrt{\omega^2+\nu_{\mathrm{en}}^2}}\cdot\cos(\omega t+\phi), \tag{3}$$

$$\vec{r} = \frac{e\vec{E}_{\mathrm{rf}}}{m\omega\sqrt{\omega^2+\nu_{\mathrm{en}}^2}}\cdot\sin(\omega t+\phi), \tag{4}$$

where $\phi = \arctan(\nu_{\mathrm{en}}/\omega)$. The amplitude, A, of the electron displacement in an rf electric field is given by

$$A = \frac{eE_{\mathrm{rf}}}{m\omega\sqrt{\omega^2+\nu_{\mathrm{en}}^2}} = \frac{V_{\mathrm{dr}}}{\omega}, \tag{5}$$

where the maximum instantaneous drift velocity of electrons, V_{dr}, is given by

$$V_{\mathrm{dr}} = \frac{eE_{\mathrm{rf}}}{m\sqrt{\omega^2+\nu_{\mathrm{en}}^2}}. \tag{6}$$

Let $U_{\mathrm{rf}} = U_{\mathrm{rf}}(p)$ be the amplitude of the rf voltage at breakdown. A minimum in the rf breakdown curve, $U_{\mathrm{rf}}(p)$, occurs when $\mathrm{d}U_{\mathrm{rf}}(p)/\mathrm{d}p = 0$, and a turning point occurs when $\mathrm{d}U_{\mathrm{rf}}(p)/\mathrm{d}p \to \infty$. At the turning point of the breakdown curve (corresponding to $p = p_{\mathrm{t}}$ and $U_{\mathrm{rf}} = U_{\mathrm{t}}$) the amplitude of the electron displacement is equal to half of the gap [25]:

$$A = \frac{V_{\mathrm{dr}}}{\omega} = \frac{L}{2}. \tag{7}$$

Hence the electron drift velocity, V_{dr}, at the turning point of the rf breakdown curve is equal to

$$V_{\mathrm{dr}} = \frac{\omega\cdot L}{2} = L\pi f. \tag{8}$$

The same equation was derived previously for the collisional regime ($\nu_{\mathrm{en}} \gg \omega$) [21–25]. Here we show that the same equation is valid for all values of ν_{en} and ω. It follows from equation (8) that the value of the electron drift velocity at the turning point of the breakdown curve depends only on the values of the inter-electrode gap and the frequency of the rf field. At the same time it is independent of the gas species. However, the corresponding value of E/p at this point will be different for each gas. The coordinates of the turning point permit us to determine the reduced field, E/p, corresponding to this electron drift velocity.

At the breakdown curve minimum (with the coordinates U_{min} and p_{min}) the following expression for the electron drift velocity was derived by Lisovskiy *et al* [25]:

$$V_{\mathrm{dr}} = \frac{\omega L}{2}\cdot\frac{B-(1/\sqrt{2})(E/p)_{\mathrm{min}}}{B+(1/\sqrt{2})(E/p)_{\mathrm{min}}}. \tag{9}$$

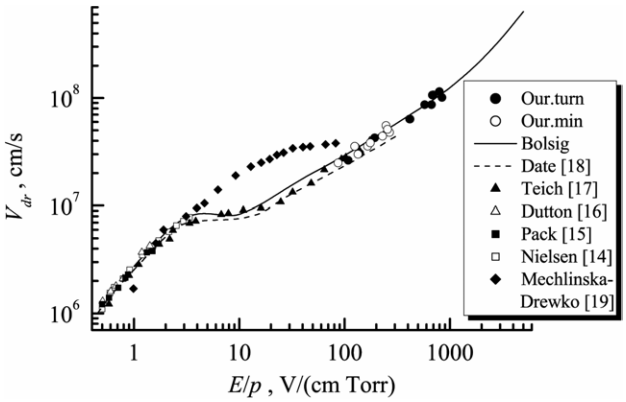

Figure 5. Electron drift velocity in N_2O against E/p. The solid curve presents the data calculated with the Bolsig code, solid circles are for our measured data (from the turning points), empty circles are for our measured data (from the minima), solid triangles are for the experimental data from [17], empty triangles are for the experimental data from [16], solid squares are for the experimental data from [15], empty squares are for the experimental data from [14] and solid diamonds are for the experimental data from [19]. The dashed curve presents the calculation data from [18].

Thus we can also determine the electron drift velocity from the measured coordinates of the rf breakdown curve minimum. A disadvantage of this technique is that it depends on knowledge of the constant B, which is related to the first Townsend coefficient α by

$$\alpha = A_1\cdot p\cdot\exp\left(-\frac{B}{E_{\mathrm{eff}}/p}\right), \tag{10}$$

where E_{eff} is the effective electric field strength, $E_{\mathrm{eff}} = E_{\mathrm{rf}}/\sqrt{2}$, A_1 and B are constants depending on the gas species. Therefore this technique can only be applied to gases for which this first Townsend coefficient is known. However, this technique enables the electron drift velocity to be determined from rf breakdown curves which show no turning point.

The coordinates of the turning point and the minimum permit us to determine the reduced field, E/p, corresponding to this electron drift velocity. For example, take the coordinates of the turning point observed in the breakdown curve for a gap of 20.4 mm (see figure 2(*c*)): $p_{\mathrm{t}} = 0.093$ Torr and $U_{\mathrm{t}} = 127$ V. Then $E/p = 669.4\,\mathrm{V\,cm^{-1}\,Torr^{-1}}$ and $V_{\mathrm{dr}} = 8.69\times10^7\,\mathrm{cm\,s^{-1}}$. The minimum for this curve occurs at the coordinates $p_{\mathrm{min}} = 0.195$ Torr and $U_{\mathrm{min}} = 89$ V, therefore $E/p = 223.7\,\mathrm{V\,cm^{-1}\,Torr^{-1}}$, and from (9) we have $V_{\mathrm{dr}} = 4.51\times10^7\,\mathrm{cm\,s^{-1}}$. Thus the measured breakdown curve for one gap value provides two values of the electron drift velocity (provided that the breakdown curve possesses a diffusion-drift branch with a well-expressed turning point). In order to obtain a set of V_{dr} values over a wide range of E/p, rf breakdown curves must be recorded at various values of the inter-electrode gap L. The rf breakdown curves for the gap $L > 12$ mm and the frequency $f = 13.56$ MHz, as well as for $f = 27.12$ MHz (presented in figure 2(*b*)), possess diffusion–drift branches with multi-valued regions; therefore we can use them to determine the electron drift velocity from the location of the turning point of the rf breakdown curve.

The values of the electron drift velocity determined from our measured breakdown curves are presented in figure 5. The

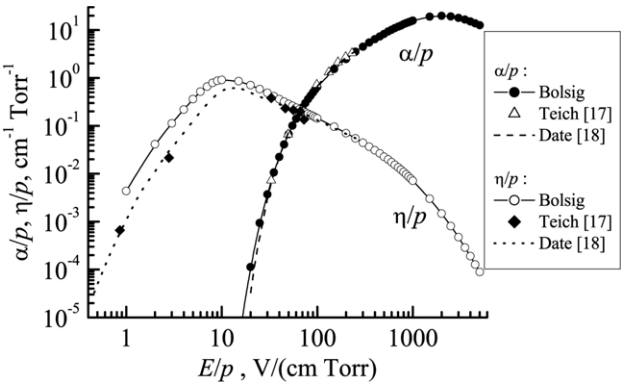

Figure 6. Ionization coefficient (the first Townsend coefficient) α/p and the attachment coefficient η/p against the value of E/p for N_2O; α/p: solid circles are for our calculated data, empty triangles are for the experimental data from [17] and the dashed curve presents the calculated data from [18]; η/p: empty circles are for our calculated data, solid diamonds are for the experimental data from [17] and dotted curve presents the calculation data from [18].

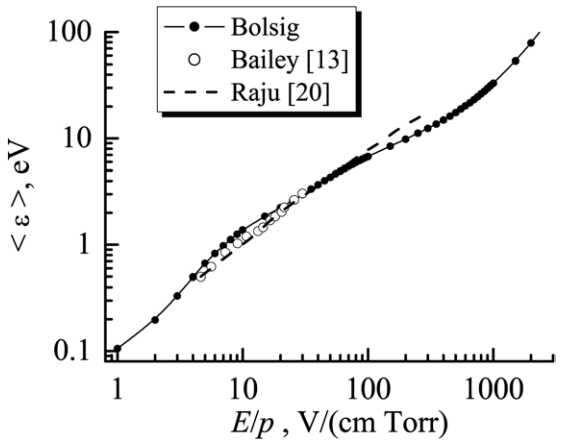

Figure 7. The average electron energy as a function of E/p: solid circles are for our calculated data, empty circles are for the experimental data from [13] and the dashed curve presents the calculation data from [20].

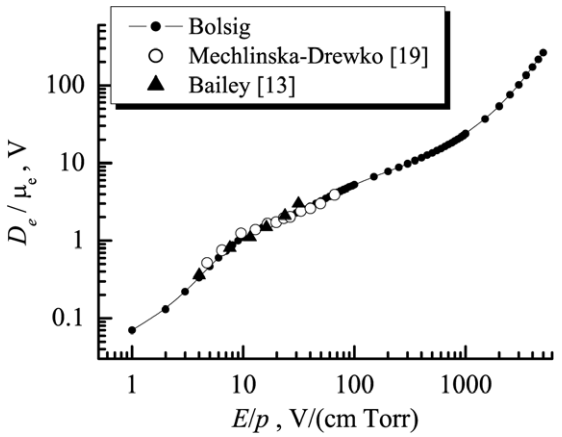

Figure 8. Ratio D_e/μ_e against E/p: the solid circles are for our calculated data, the empty circles are for the experimental data from [19] and the solid triangles are for the experimental data from [13].

same figure shows previous measurements in the literature [14–17, 19], as well as the results of calculations [18]. However, while Teich [17] recorded the electron drift velocity up to $E/p \leqslant 174\,\mathrm{V\,cm^{-1}\,Torr^{-1}}$, and Date *et al* [18] calculated it up to $E/p = 322\,\mathrm{V\,cm^{-1}\,Torr^{-1}}$, we determined the electron drift velocity over the range $E/p = 87$–$840\,\mathrm{V\,cm^{-1}\,Torr^{-1}}$. It is clear from figure 5 that our data are in good agreement with these two previous studies in the range $E/p = 87$–$322\,\mathrm{V\,cm^{-1}\,Torr^{-1}}$. However for higher E/p values there are no data in the literature. The only other measurements of the drift velocity [14–16] were performed only for $E/p \leqslant 4\,\mathrm{V\,cm^{-1}\,Torr^{-1}}$, so it is unreasonable to compare our results with this data. We therefore compared our results with calculated values derived from the cross-sections of Hayashi and Niwa [26] using the Bolsig code (www.siglo-kinema.com/bolsig.htm). Bolsig is a code for the numerical solution of the Boltzmann equation for electrons in weakly ionized gases and in steady-state, uniform fields. This code was designed to generate electron transport data in pure gases or gas mixtures.

3.2.1. Calculated electron transport parameters. The Bolsig code can be used to calculate electron transport parameters in the electric field in the range $E/p \geqslant 1\,\mathrm{V\,cm^{-1}\,Torr^{-1}}$ for 15 different gases and their mixtures but does not contain N_2O. Earlier [24] we added ammonia to this list of gases. Here we have added the cross-sections for elastic and inelastic collisions of electrons with N_2O molecules presented by Hayashi and Niwa [26] to the set of cross sections for this Bolsig code, extending the set of gases to 17.

Figure 5 shows the calculated values of the electron drift velocity for N_2O over the range $E/p = 1$–$5000\,\mathrm{V\,cm^{-1}\,Torr^{-1}}$ together with our measured data. It is clear that the values are in good agreement. There is also good agreement between the calculated values and the previous measurements [14–17, 19] at low E/p.

Figure 6 presents the dependence of the first Townsend coefficient (ionization coefficient) α/p and the attachment coefficient η/p as a function of E/p for N_2O (the latter process leads to the dissociation of the N_2O molecule into a neutral nitrogen molecule and a negative oxygen ion). The calculated data for α/p coincide with previous measured [17] and calculated [18] data. The values of the attachment coefficient, η/p, we obtained are in satisfactory agreement with previous experimental [17] and calculated [18] data.

Figure 7 shows the calculated dependence of the average electron energy, $\langle\varepsilon_e\rangle$ on the reduced field, E/p, which is in satisfactory agreement with previous experimental [13] and calculated [20] values. Figure 8 presents the ratio of radial electron diffusion coefficient to the mobility, D_e/μ_e, as a function of E/p obtained using the Bolsig code, giving satisfactory agreement with previous experimental data [13, 19].

4. Conclusions

We have determined the electron drift velocity in N_2O from the location of the turning points and minima of the breakdown curves of rf capacitive gas discharges over the range $E/p = 87$–$840\,\mathrm{V\,cm^{-1}\,Torr^{-1}}$. With the help of the numerical Bolsig

code and published cross-sections we have calculated the electron transport parameters (electron drift velocity, V_{dr}, the first Townsend coefficient, α, the rate of electron attachment to gas molecules, η, the average electron energy, $\langle\varepsilon_e\rangle$, the ratio of radial electron diffusion coefficient to mobility, D_e/μ_e) in N_2O in the range $E/p = 1$–$5000\,\mathrm{V\,cm^{-1}\,Torr^{-1}}$. The values of the drift velocity obtained from the experiment are in good agreement with the calculated data.

Acknowledgments

The authors express their gratitude to the Displays Division of Unaxis France, Palaiseau for their financial support and for the equipment used in this study.

References

[1] Lee D R, Lucovsky G, Denker M S and Magee C 1995 *J. Vac. Sci. Technol.* A **13** 1671
[2] Kaluri S R and Hess D W 1998 *J. Electrochem. Soc.* **145** 662
[3] Campmany J, Andujar J L, Canillas A, Costa J and Bertran E 1993 *Appl. Surf. Sci.* **70–71** 695
[4] Campmany J, Canillas A, Andujar J L, Costa J and Bertran E 1993 *Thin Solid Films* **228** 137
[5] Scopel W L, Cuzinatto R R, Tabacniks M H, Fantini M C A, Alayo M I and Pereyra I 2001 *J. Non-Cryst. Solids* **288** 88
[6] Alayo M I, Pereyra I, Scopel W L and Fantini M C A 2002 *Thin Solid Films* **402** 154
[7] Scopel W L, Fantini M C A, Alayo M I and Pereyra I 2002 *Thin Solid Films* **413** 59
[8] Kaganowicz G, Ban V S and Robinson J W 1984 *J. Vac. Sci. Technol.* A **2** 1233
[9] Kushner M J 1993 *J. Appl. Phys.* **74** 6538
[10] Courtney C H, Smith B C and Lamb H H 1998 *J. Electrochem. Soc.* **145** 3957
[11] Park Y-B and Rhee S-W 1999 *J. Appl. Phys.* **86** 1346
[12] Bandet J, Despax B, Caumont M and Date L 2000 *Japan. J. Appl. Phys.* B **39** L141
[13] Bailey V A and Rudd J B 1932 *Phil. Mag.* **14** 1033
[14] Nielsen R A and Bradbury N E 1937 *Phys. Rev*. **51** 69
[15] Pack J L, Voshall R E and Phelps A V 1962 *Phys. Rev*. **127** 2084
[16] Dutton J, Gallagher J W, Beaty E C and Pitchford L C 1982 *J. Phys. Chem. Ref. Data* **22** 203
[17] Teich T H 1991 *Int. Conf. on Phenomena Ion. Gases (Pisa) XX* vol 5, ed V Palleshi and M Vaselli (Pisa: Instituto di Fisica) p 442
[18] Date L, Radouane K, Despax B, Yousfi M, Caquineau H and Hennad A 1999 *J. Phys. D: Appl. Phys.* **32** 1478
[19] Mechlinska-Drewko J, Wroblewski T, Petrovic Z Lj, Novakovic V and Karwasz G P 2003 *Radiat. Phys. Chem.* **68** 205
[20] Govinda Raju G R and Hackam R 1981 *J. Appl. Phys*. **52** 3912
[21] Lisovskiy V A 1998 *Tech. Phys. Lett.* **24** 308
[22] Lisovskiy V A and Yegorenkov V D 1998 *J. Phys. D: Appl. Phys*. **31** 3349
[23] Lisovskiy V A and Yegorenkov V D 1999 *J. Phys. D: Appl. Phys.* **32** 2645
[24] Lisovskiy V, Martins S, Landry K, Douai D, Booth J-P and Cassagne V 2005 *J. Phys. D: Appl. Phys.* **38** 872
[25] Lisovskiy V, Booth J-P, Landry K, Douai D, Cassagne V and Yegorenkov V 2006 *J. Phys. D: Appl. Phys.* **39** 660
[26] Hayashi M and Niwa A 1987 *Gaseous Dielectrics V* ed L G Christophorou and D W Bouldin (New York: Pergamon) p 27
[27] Levitskii S M 1957 *Sov. Phys.—Tech. Phys*. **2** 887
[28] Lisovskiy V, Martins S, Landry K, Douai D, Booth J-P, Cassagne V and Yegorenkov V 2005 *Phys. Plasmas* **12** 093505
[29] Smith H B, Charles C and Boswell R W 2003 *Phys. Plasmas* **10** 875
[30] Githens S 1940 *Phys. Rev*. **57** 822
[31] Chenot M 1948 *Ann. Phys., Paris* **3** 277
[32] Hatch A J and Williams H B 1958 *Phys. Rev.* **112** 681
[33] Gilardini A L 1995 *J. Appl. Phys.* **78** 783
[34] Kishek R A, Lau Y Y and Chernin D 1997 *Phys. Plasmas* **4** 863
[35] Udiljak R, Anderson D, Lisak M, Semenov V E and Puech J 2004 *Phys. Plasmas* **11** 5022
[36] Paschen F 1889 *Ann. Phys. Chem.* **37** 69
[37] Lisovskiy V A, Yakovin S D and Yegorenkov V D 2000 *J. Phys. D: Appl. Phys.* **33** 2722
[38] Brown S C 1956 *Encyclopedia of Physics* ed S Flugge (Berlin: Springer) p 546
[39] Lisovskiy V, Booth J-P, Martins S, Landry K, Douai D and Cassagne V 2005 *Europhys. Lett.* **71** 407